Atmos. Chem. Phys. Discuss., 13, 19009–19049, 2013
www.atmos-chem-phys-discuss.net/13/19009/2013/
doi:10.5194/acpd-13-19009-2013

Atmospheric Chemistry and Physics Discussions

Characterization of submicron aerosols during a serious pollution month in Beijing (2013) using an aerodyne high-resolution aerosol mass spectrometer

J. K. Zhang[1,2], Y. Sun[1], Z. R. Liu[1], D. S. Ji[1], B. Hu[1], Q. Liu[1], and Y. S. Wang[1]

[1]State Key Laboratory of Atmospheric Boundary Layer Physics and Atmospheric Chemistry (LAPC), Institute of Atmospheric Physics, Chinese Academy of Sciences, Beijing 100029, China
[2]University of Chinese Academy of Sciences, Beijing 10049, China

Received: 23 May 2013 – Accepted: 25 June 2013 – Published: 16 July 2013

Correspondence to: Y. S. Wang (wys@dq.cern.ac.cn)

Published by Copernicus Publications on behalf of the European Geosciences Union.

Abstract

In January 2013, Beijing experienced several serious haze events. To achieve a better understanding of the characteristics, sources and processes of aerosols during this month, an Aerodyne High-Resolution Time-of-Flight Aerosol Mass Spectrometer (HR-ToF-AMS) was deployed at an urban site between 1 January and 1 February 2013 to obtain the size-resolved chemical composition of non-refractory submicron particles (NR-PM_1). During this period, the mean measured NR-PM_1 mass concentration was 87.4 $\mu g\,m^{-3}$ and was composed of organics (49.8 %), sulfate (21.4 %), nitrate (14.6 %), ammonium (10.4 %), and chloride (3.8 %). Moreover, inorganic matter, such as sulfate and nitrate comprised an increasing fraction of the NR-PM_1 load as NR-PM_1 loading increased, denoting their key roles in particulate pollution during this month. The average size distributions of the species were all dominated by an accumulation mode peaking at approximately 600 nm in vacuum aerodynamic diameter and organics characterized by an additional smaller size (~ 200 nm). Elemental analyses showed that the average O/C, H/C, and N/C (molar ratio) of organic matter were 0.34, 1.44 and 0.015, respectively, corresponding to an OM/OC ratio (mass ratio of organic matter to organic carbon) of 1.60. Positive matrix factorization (PMF) analyses of the high-resolution organic mass spectral dataset differentiated the organic aerosol into four components, i.e., oxygenated organic aerosols (OOA), cooking-related (COA), nitrogen-containing (NOA) and hydrocarbon-like (HOA), which on average accounted for 40.0, 23.4, 18.1 and 18.5 % of the total organic mass, respectively. Back trajectory clustering analyses indicated that the WNW air masses were associated with the highest NR-PM_1 pollution during the campaign. Aerosol particles in southern air masses were especially rich in inorganic and oxidized organic species, whereas northern air masses contained a large fraction of primary species.

ACPD
13, 19009–19049, 2013

1 Introduction

Beijing is one of the most economically developed regions in China, with a population of more than 20 million and a vehicle fleet of approximately 500 million (Beijing Municipal Bureau of Statistics). The rapid development of a variety of industries such as power plants, industrial production, and transportation has resulted in a high emission rate of particulate matter (PM). The most serious PM pollution of this century appeared in January 2013. The highest instantaneous concentration of $PM_{2.5}$ reached 1000 $\mu g\,m^{-3}$ in some heavily polluted areas of Beijing. The affected population was up to 0.8 billion in China. The fine particle concentration also reached a high level during this serious pollution month. As is well-known, compared with coarse particles, fine particles can penetrate deeply into the lung, leading to adverse effects on human health. Meanwhile, these particles have important effects on visibility, climate forcing, and the deposition of acids and nutrients to ecosystems and crops (Ulbrich et al., 2009). However, fine particles are still not well-understood in China, because it is difficult to deeply understand their variation in chemical and physical properties due to their heterogeneous distribution and short atmospheric lifetimes (Mohr et al., 2011).

In addition to the complexity of fine particles, our level of understanding of the nature, sources, processes and effects of fine particles is currently limited by the instrumentation that is available to study them. Most previous aerosol studies have been based on filter samplings followed by laboratory analyses. These methods typically have a time resolution of a few hours to days, are limited by both the minimum amount of material that is required to be collected for analysis and labor and analysis costs, and cannot capture many dynamic changes of aerosol size distributions and chemical composition that occur over faster timescales (Ge et al., 2012). Recent studies performed in some countries have demonstrated that the chemical compositions of fine particles can be significantly altered on a time scale of hours to days in regions strongly affected by anthropogenic sources (Takegawa et al., 2006; Volkamer et al., 2006; Brock et al., 2008). In contrast, real-time measurements of size-resolved chemical compositions can be

ACPD
13, 19009–19049, 2013

performed using aerosol mass spectrometry. Aerosol mass spectrometers (AMS) have become a widely applied tool because they allow for chemical speciation and for the sizing and mass detection of submicron non-refractory PM at a high time resolution (Canagaratna et al., 2007; Mohr et al., 2012). Three versions of the AMS (Q-AMS, C-ToF-AMS, and HR-ToF-AMS) are currently employed. The application of HR-ToF-AMS for ambient studies is relatively new and started only in recent years (DeCarlo et al., 2006). Compared to Q-AMS and C-ToF-AMS, HR-ToF-AMS is significantly improved in terms of chemical resolution and sensitivity. In particular, the high m/z resolution of the HR-ToF-AMS allows for most ion fragments, especially those at low m/z's (< 100), to be resolved and for their nominal elemental compositions (i.e., ratios among carbon (C), hydrogen (H), oxygen (O), and nitrogen (N) of OA to be determined) (Aiken et al., 2008; Sun et al., 2011).

Over the last decade, many aerosol studies have also revealed that organic aerosol (OA) is the most abundant component of fine particles, and that it makes up a large fraction (20 to 90 %) of the submicron particulate mass (Zhang et al., 2007a; Murphy et al., 2006). They are the sum of multiple primary and secondary sources that can evolve due to aging processes. Correctly apportioning organic aerosols into their sources and components is a critical step towards enabling efficient control strategies and model representations (Ulbrich et al., 2009). However, knowledge about sources and the fate and mutual interaction of gas phase and aerosol organics, of which it is estimated that there are between 10 000 and 100 000 different compounds, is still limited (Goldstein and Galbally, 2007). This information is also needed to elucidate the climate and health impacts of aerosols (Ghan and Schwartz, 2007). Therefore, the atmospheric evolution of organic aerosol (OA) is the focus of intense research activities (Jimenez et al., 2009). Recently, AMS data have been combined with positive matrix factorization (Ulbrich et al., 2009; Lanz et al., 2007), a factor analysis model that outputs a number of constant source profiles (factors) and their varying contributions over time, which has led to new insights into sources contributing to OA (Mohr et al., 2012). Based on the AMS measurements, hydrocarbon-like OA (HOA) from traf-

ACPD
13, 19009–19049, 2013

fic, biomass burning OA (BBOA), and oxygenated OA (OOA) have been distinguished in many datasets where secondary organic aerosol (SOA) is assumed to be the main contributor to OOA (Jimenez et al., 2009; Lanz et al., 2010). OOA can be further separated into a low volatility fraction (LV-OOA), which is more aged and exhibits a higher O : C ratio, and a semi-volatile fraction (SV-OOA) which represents fresher OOA with a lower O : C ratio, in some studies (Lanz et al., 2007; Aiken et al., 2008; Huang et al., 2010; Huang et al., 2011; Mohr et al., 2012).

Although it is the capital of China and one of the most air-polluted cities in the world, there are currently only several reports focused on fine particles in Beijing. These studies have revealed that their major chemical components include organic matter (OM), sulfate, nitrate and ammonium. The major sources of these fine particles include vehicular emissions, coal and biomass burning and secondary formations (Huang et al., 2006; Song et al., 2006; Streets et al., 2007). Sun et al. (2010) recently reported highly time-and size-resolved fine particle measurement results in Beijing for the summer of 2006 using a Q-AMS. Huang et al. (2010) used an HR-ToF-AMS to characterize submicron aerosol particles during the period of the 2008 Beijing Olympic Games and Paralympic Games. These in situ high-time resolution measurements have provided more information on the variability in fine particle chemistry and microphysics than off-line filter samplings.

For this study, we deployed a High-Resolution Time-of-Flight Aerosol Mass Spectrometer (HR-ToF-AMS or simply AMS) manufactured by Aerodyne Research Inc. (Billerica, MA, USA) in urban Beijing to measure airborne submicron particles with a high-time resolution during this month of serious pollution. The main findings include (1) mass concentrations, size distributions, chemical composition, and temporal and diurnal variations of NR-PM_1 species; (2) the elemental composition of the OA; and (3) characteristics and dynamic variations of the OA components determined via positive matrix factorization (PMF) of the high-resolution mass spectra (HRMS).

ACPD
13, 19009–19049, 2013

2 Experimental methods

2.1 Sampling site description

AMS measurements were performed continuously between 1 January and 1 February 2013 at the Institute of Atmospheric Physics (IAP), Chinese Academy of Sciences (CAS), to measure the on-line chemical compositions and size distributions of the NR-PM_1 aerosol components. The observation site is located between the north 3rd Ring Road and north 4th Ring Road. The site is approximately 1 km from the 3rd Ring Road, 200 m from the Badaling Highway running north-south to its east, and 50 m from the Beitucheng West Road running east-west to its north. Ambient air was sampled at approximately 15 m above ground.

At the same time, an automatic meteorological observation instrument (Milos520, Vaisala, Finland) was located at the 8 m level and was used to observe the main meteorological parameters, including temperature, humidity, and the speed and direction of wind in the atmosphere at ground level. The datasets for NO_x were acquired from the Beijing–Tianjin–Hebei Atmospheric Environment Monitoring Network.

2.2 HR-ToF-AMS measurement and data processing

2.2.1 HR-ToF-AMS operation

The AMS mass spectrum was scanned from m/z 12 to 596, and the sampling flow rate was 90 mL min^{-1}. A detailed description of the instrument can be found in DeCarlo et al. (2006). During this campaign, the AMS was operated under the "V" and "W" ion optical modes alternatively every 7.5 min. The V-mode is more sensitive, whereas the W-mode has a higher mass resolution. Under V-mode operation, the AMS cycled through the mass spectrum (MS) mode and the particle time-of-flight (PToF) mode every 45 s, spending 22.5 s for open and closed status under MS mode, respectively. Size distribution data are reported in units of mass-weighted aerodynamic diameter.

ACPD
13, 19009–19049, 2013

No PToF data were sampled in W-mode due to the limited signal-to-noise (S/N) ratio. However, the high mass resolution (~ 5000–6000) of W-mode allows us to determine the ion-specific mass spectra and, thus, the elemental compositions of OA (DeCarlo et al., 2006; Aiken et al., 2008).

The AMS was calibrated for inlet flow, ionization efficiency (IE), and particle sizing at the beginning, middle and end of the campaign following standard protocols (Jayne et al., 2000; Jimenez et al., 2003; Drewnick et al., 2005). The calibration of the IE was conducted using size-selected pure ammonium nitrate particles and the calibration for particle size was conducted using mono-disperse polystyrene latex spheres. The detection limit of the individual species was determined as three times the standard deviation of the corresponding signal in particle-free air (DeCarlo et al., 2006; Sun et al., 2009). As a result, the 5 min DLs of organics, sulfate, nitrate, ammonium, and chloride were 0.056, 0.006, 0.008, 0.04 and 0.014 $\mu g\,m^{-3}$, respectively.

2.2.2 HR-ToF-AMS data analysis

The mass concentrations and size distributions of the species measured with the AMS were calculated using methods outlined in DeCarlo et al. (2006). Standard ToF-AMS data analysis software packages (SQUIRREL version 1.50 and PIKA version 1.09) downloaded from the ToF-AMS-Resources webpage (http://cires.colorado.edu/jimenez-group/ToFAMSResources) were used to generate unit and high-resolution mass spectra from the V-mode and W-mode data, respectively (Huang et al., 2010; He et al., 2011). SQUIRREL employs a user-definable fragmentation table to apportion the total signals into different species (Allan et al., 2004). PIKA employs a peak-shape modified Gaussian-fitting algorithm to deconvolve and quantify the signals of a user-defined array of ions (DeCarlo et al., 2006). The V-mode and PToF data were processed with SQUIRREL to determine the mass concentrations and size distributions of the NR-PM_1 species. The W-mode data were processed with PIKA to obtain high-resolution mass spectra and the elemental composition of the organic species.

ACPD
13, 19009–19049, 2013

According to the results of Liu et al. (2011), a collection efficiency (CE) factor of 0.5 was used to account for the incomplete detection of aerosol species due to particle bounce at the vaporizer and/or the partial transmission of particles by the lens. Previous studies have demonstrated that an AMS CE = 0.5 is a good assumption in many cases, especially under dry conditions (Allan, 2004; Takegawa et al., 2005). In this study, to reduce the uncertainties of CE due to particle phase water, a silica gel diffusion dryer was introduced to keep the relative humidity in sampling line below 40 %. The relative ionization efficiency (RIE) values used in this study were 4.0 for ammonium, 1.2 for sulfate, 1.1 for nitrate, 1.3 for chloride and 1.4 for organics (Jimenez et al., 2003).

Positive matrix factorization (PMF) (Paatero and Tapper, 1994) analyses were performed on the HRMS, i.e., the ion-speciated W-mode spectra, using the PMF Evaluation Toolkit (PET) v2.05 (Ulbrich et al., 2009). The HRMS data and error matrices were generated as outlined in DeCarlo et al. (2010). Data and error matrices were first generated in PIKA. We took into account ions up to m/z 120, given that larger ions had a low signal/noise ratio and were more biased because of an insufficient mass resolution. Isotopes were systematically constrained in PIKA but were removed from the data and error matrices because their presence would have given excess weight to the parent ions in the PMF analysis (Setyan et al., 2012). Ions with S/N ratio < 0.2 were removed from the HRMS data and error matrices before the PMF analysis. The "weak" ions with S/N between 0.2 and 2 were downweighted by increasing their errors by a factor of 2 (Paatero and Hopke, 2003; Ulbrich et al., 2009). More technical details of the PMF analysis can be found in other recent publications (Huang et al., 2010).

The PMF analysis based on the HRMS dataset observed in the campaign was performed for 1 to 8 factors. In the PMF analysis, the Q/Q_{exp} values represent the ratios between the actual sum of the squares of the scaled residuals (Q) obtained from the PMF least square fit and the ideal Q (Q_{exp}) obtained if the fit residuals at each point were equal to the noise specified for each data point. The Q/Q_{exp} values of greater than the ideal value of 1 may be indicative of the fact that the input noise values underestimate the true noise because they do not include errors associated with the

ACPD
13, 19009–19049, 2013

highresolution peak fitting process (He et al., 2011). In a 1 or 2 factor solution, the residual at the key m/z's and time periods were too large. Meanwhile, the Q/Q_{exp} values were too high, 10.4 and 7.5 respectively. In the 3 factor solution, the Q/Q_{exp} decreased (6.1). We identified three components, including oxygenated organic aerosols (OOA), cooking-related (COA) and hydrocarbon-like (HOA), whereas there were many nitrogen-containing fragments in the MS of the OOA (N/C is 0.023) and HOA (N/C is 0.028) and the time trends and diurnal cycles of them mixed with each other. In the 4 factor solution, the Q/Q_{exp} was 5.0 and a new component was identified. The MS of this new component contained many nitrogen-containing fragments, and the N/C value was 0.059. The N/C values for OOA and HOA then dropped to 0.009 and 0.010, respectively. Moreover, the diurnal cycles of the four components were distinctive, and the element ratios of these components were within a reasonable range compared with other studies. In the 5 factor solution, the Q/Q_{exp} was 4.9, and tow OOA components appeared. The MS characteristics of these components and their diurnal cycles were similar. In addition, the contribution of this component to the OA was only 6 %. Moreover, many studies have determined that the OOA component cannot be separated into different OOAs due to the lower temperature and the smaller (diurnal) temperature ranges during winter (Jimenez et al., 2009; Allan et al., 2010). Therefore, the number of factors is 5, which is not a reasonable result. When the number of factors changed from 6 to 8, there was not an obvious decrease of the Q/Q_{exp} value and some of the split factors had time series and MS that appeared mixed. Thus, the four factor solution was chosen as the optimal solution. The sensitivity of the 4 factor solution to rotation and starting values was explored by varying the FPEAK and seed parameters. Lower Q/Q_{exp} values can indicate a better fit to the data set and thus be used as one criterion for choosing a suitable solution (Ulbrich et al., 2009). With FPEAK varying from −1.5 to 1.5 in increments of 0.2 (seed = 0), the lowest Q/Q_{exp} was obtained at approximately 0. Therefore, FPEAK = 0 was chosen as the best solution. With a seed value varying from 0 to 250 in increments of 10 (FPEAK = 0), the Q/Q_{exp} almost had no change.

ACPD
13, 19009–19049, 2013

Based on all of these tests, the four factor, FPEAK = 0, seed = 0 solution was chosen as the optimal solution for this analysis.

An elemental analysis of the HRMS data for C, H, O, and N time series and ratios was performed using the APES v1.05 software within Igor Pro 6.21A.

3 Results and discussion

3.1 Submicron aerosol characteristics

Figure 1 presents the time-resolved variation of organic, nitrate, sulfate, ammonium, and chloride mass concentrations measured with the AMS and meteorological parameters (e.g., temperature, RH, wind speed and direction) from 1 January to 1 February 2013.

The meteorological conditions during the campaign are presented in Fig. 1a and b. The temperature had clear diurnal cycles, with higher values observed during the daytime. Relative humidity had peak values during the night. During the campaign, the temperature varied from −12.1 °C to 4.6 °C, with a campaign average of −2.8 °C. Relative humidity was in the range of 11 to 92 %, averaging 49 %. Wind speed varied from 0 m s^{-1} to 8.1 m s^{-1} with an average of 1.5 m s^{-1} during the sampling period.

Figure 1c and d present the time series for the NR-PM$_1$ species mass concentration and NR-PM$_1$ components during the campaign. Several serious pollution events occurred during the month. Therefore, the range of NR-PM$_1$ mass concentrations was broad (from 3.1 to 406 µg m^{-3} was observed, the mean mass concentration was 87.4 µg m^{-3}). These values are much higher than those observed in developed countries, such as 11.0 µg m^{-3} in New York in 2009 (Sun et al., 2011) and 14.8 µg m^{-3} in Pittsburgh in 2002 (Zhang et al., 2005a). In addition, these values are also higher compared to other results measured in Beijing in 2006 (80.0 µg m^{-3}) by Sun et al. (2010) and in 2008 (61.1 µg m^{-3}) by Huang et al. (2010). Like the total mass, all the species also varied significantly. Organics, for example, sometimes reached as high as over

ACPD
13, 19009–19049, 2013

180 $\mu g\,m^{-3}$ and as low as less than 2 $\mu g\,m^{-3}$. Figure 1c and d also show that different species exhibit different trends as the total mass concentrations increased, i.e., the relative contribution of organics displayed a significant decreasing trend, whereas the inorganic displayed a significant increasing trend, especially for sulfate and nitrate. During the most serious pollution event (from 00:00 on 25 January to 12:00 on 1 February), the relative contribution of organics decreased from 73.9 to 39.8 %, whereas the contribution of nitrate and sulfate increased from 6.6 and 10.3 to 20.6 % and 25.1 % from the start of the event (period I) to the highest concentration (period II), respectively, although the mass concentrations of all species increased. However, the contribution of organics obviously increased when the NR-PM_1 decreased at the end of this event (period III).

Figure S1 shows the time series for the NR-PM_1 concentrations measured by AMS and a tapered element oscillating microbalance (TEOM, Rupprecht & Patashnick Co., Inc, model 1400A, Albany, New York) that sampled at 50° and that was equipped with a Nafion diffusion dryer sample equilibration system (SES) along with a PM_1 inlet. The two measurements are highly correlated, with a linear correlation coefficient (R^2) of 0.73 and a slope of 0.85 (Fig. S2).

Meteorological factors had decisive roles during periods when the atmosphere became stagnant and stable and pollution levels increased, an accumulation process, and also when pollution levels decreased during the dispersion and removal ("cleanup") process. During the accumulation process, the wind was light and variable. However, during the cleanup process, the surface and transport wind speeds obviously increased and the atmosphere became less stable, thus diluting the NR-PM_1 mass concentrations in Beijing. The most obvious and rapid cleanup processes occurred on 8 and 24 January though there were several other such periods as well. In addition, the relative humidity was also important for the pollution event. A higher humidity is conducive to the formation of sulfate and nitrate pollutants. During this same pollution event, in which we discussed the changes in the relative contributions of all species, there were obvious changes in the meteorological factors during the three periods. During periods

ACPD
13, 19009–19049, 2013

I and II, the average wind speed value was only 1.1 $m s^{-1}$, and the temperature and relative humidity increased, and becoming stable under a temperature inversion during period II. Under these types of conditions, pollutants will accumulate and form a significant amount of secondary pollutants, such as sulfate and nitrate, which is why their contributions obviously increased during period II. However, during period III, the wind speed reached 3.2 $m s^{-1}$, and the temperature and relative humidity decreased. The NR-PM_1 mass concentration also obviously decreased during this period.

As shown in Fig. 1e, on average, organics were the most abundant NR-PM_1 species, accounting for 49.8 % of the total mass, followed by sulfate (21.4 %), nitrate (14.6 %), ammonium (10.4 %), and chloride (3.8 %). This contribution of organics is higher than for previous observations in Beijing, such as in 2006 (35 %) (Sun et al., 2010) and 2008 (37.9 %) (Huang et al., 2010), whereas the contribution of sulfates is similar or lower than these years (22 and 26.7 %, respectively). However, the contribution of organics is lower compared to some foreign cities, such as New York (54 %) (Sun et al., 2011) and Whistler Mountain (55 %) (Sun et al., 2009). We must note that black carbon was included in Beijing for 2008 and in New York for 2009. Therefore, this analysis needs to exclude the contribution of BC. The contribution of BC in 2008 was only 3.1 %, a small effect in the comparison. On the other hand, we recalculated the contribution of every species from the New York research study on the basis of the data table (excluding the BC), which was provided in the paper. Therefore, the results are reasonable.

As the ambient NR-PM_1 mass concentration during the campaign varied significantly, it is interesting to examine the relative contributions of different species at different total mass concentrations (Huang et al., 2010). Figure 1f shows that different species exhibit different trends as the total mass concentrations increased. The percent contributions of organics displayed a decreasing trend from 62.7 % at 0–10 $\mu g m^{-3}$ to 41.1 % at > 400 $\mu g m^{-3}$. Conversely, the percent contributions of other components displayed a notable increasing trend as a function of NR-PM_1 mass loading, especially nitrate and sulfate, varying from 9.8 and 16.0 % at 0–10 $\mu g m^{-3}$ to 19.3 and 24.6 % at > 400 $\mu g m^{-3}$, respectively.

ACPD
13, 19009–19049, 2013

Figure 1g presents the average species' mass-size distributions, determined by the AMS, during the campaign. Generally, all species showed an apparent accumulation mode peaking at a relatively large size (600 nm), which is indicative of an aged regional aerosol (Alfarra et al., 2004). The very similar size distribution patterns for sulfate, nitrate and ammonium suggest they were likely internally mixed and came from similar gas-to-particle processes. However, organics also showed an additional mass distribution at smaller sizes (~ 200 nm), suggesting a significant input of fresh primary organic aerosols. Therefore, the contribution of organics to the total mass was more and more important with the decreasing size. Alfarra et al. (2004) found that the small organic mode at the urban site was well correlated with gas phase CO, 1,3-butadiene, benzene and toluene with Pearson's r values of 0.76, 0.71, 0.79 and 0.69, respectively, suggesting that combustion-related emissions are likely to be the main source of the small organic mode at this site. Xiao et al. (2009) also suggested that combustion-related emissions (e.g., traffic emissions) are likely the main source of the smaller mode. An enrichment of organics at smaller sizes was also observed in other urban AMS measurements (Aiken et al., 2009; Huang et al., 2010). It should also be noted that the transmission efficiency of the AMS inlet is typically 30–50 % at Dva = 1000 nm, depending on the exact details of the lens assembly and sampling pressure (Takegawa et al., 2009). Therefore, the aerosol size distribution patterns reported here might miss some particle mass at Dva > 600 nm.

3.2 Diurnal variation of NR-PM_1 species

The diurnal variation patterns are affected by the emission sources, photochemical reactions, meteorological conditions and the boundary layer height. Figure 2 presents the diurnal variation patterns of different NR-PM_1 species in the form of box plots. Different species presented different diurnal trends during this campaign. Because organics have both large primary and secondary origins and are also influenced by semi-volatility, the observed diurnal pattern of the organics was a complicated result (Huang et al., 2012). In this study, organics showed two broad peaks at noon (12:00–14:00)

ACPD
13, 19009–19049, 2013

and in the evening (18:00–24:00), with the second peak being much larger and the duration longer than at noon. The noon period and the period from 18:00–20:00 are the peak dining period. Meanwhile, the height of the mixing layer is lower in the evening, conducive for the accumulation of pollutants in the atmosphere. The dual role of cooking emissions and a lower mixing layer result in the higher organic concentration and a longer duration in the evening. This trend is similar to other studies in Beijing (Sun et al., 2010; Huang et al., 2010). However, this trends is unlike situations observed in other foreign urban locations, e.g., Pittsburgh (Zhang et al., 2005a) and New York City (Drewnick et al., 2004), where a morning peak of organics that correlates with morning traffic is typically observed.

There was an obvious increase in the concentration of nitrates in the afternoon, suggesting that the amount of its secondary production overwhelms its evaporation into gaseous HNO_3 and its dilution by the higher mixing layer in the afternoon, reflecting the fact that traffic emissions are typically an important source of nitrate aerosols in urban areas. However, there are many researchers that have reported contrary results, with the lowest concentrations of nitrate observed in the afternoon (He et al., 2011; Huang et al., 2011; Huang et al., 2010). For less-volatile secondary sulfate, daytime photochemical production might compensate for the daytime dilution effect and make their concentration level relatively stable during the entire day. This stable trend was also observed in Beijing in 2008 (Huang et al., 2010) and in the Pearl River Delta of China (Huang et al., 2011). The diurnal variation of ammonium was a combined result of particulate $(NH_4)_2SO_4$ and NH_4NO_3, and the diurnal trend were similar for nitrate. The observed diurnal profile of chloride, which peaks in the early morning and stays at low levels during the daytime till 07:00, was likely partially driven by the gas-particle partitioning of ammonium chloride precursors (i.e., gaseous HCl and NH_3), which is favored by the lower temperature and higher RH during the night and in the early morning. This result is consistent with Sun et al. (2010).

ACPD
13, 19009–19049, 2013

3.3 Elemental composition of organic aerosols

The HRMS obtained in this study enabled the investigation of the molecular ratios of C, H, O and N in the organic aerosol. Figure 3a and b show the variations of the atomic ratios of H/C, N/C and O/C and the mass ratios of the OM/OC of OA (organic aerosol) during this campaign. The H/C ratio varies in the range of 1.33–1.68, with a mean value of 1.44 ± 0.05, whereas the O/C ratio varies in a range of 0.14–0.58, with a mean value of 0.34 ± 0.08. The O/C atomic ratio has been regarded as a good reference for oxidation state and the photochemical age of OA (Jimenez et al., 2009; Ng et al., 2010). This value is lower than that observed at Kaiping (0.47), a rural site downwind of the central PRD area that receives pollutants through regional transport (Huang et al., 2011). This difference indicates that the pollutants emitted in an urban area become much more aged during the transport process, whereas this value is generally similar to those observed in Beijing (0.33) (Huang et al., 2010), Shenzhen (0.30) (He et al., 2011), Mexico City (0.38) (Aiken et al., 2009) and New York (0.36) (Sun et al., 2011). The N/C ratio ranges between 0.005 and 0.026, with a mean value of 0.015 ± 0.004.

The OM/OC varied between 1.33 and 1.92 during this campaign, with an average of 1.60 ± 0.11. This mass ratio has been extensively used to convert organic carbon mass to organic matter mass in filter-based aerosol chemistry studies. The OM/OC correlated well with the O/C (R^2 = 0.99, Fig. S3). The mean OM/OC value in Beijing is consistent, with a value of 1.60 (±0.2), suggesting an urban aerosol (Turpin and Lim, 2001), and the results in Shenzhen (1.57) (He et al., 2011) and New York (1.62) (Sun et al., 2011).

Figure 3c and d present the average diurnal variations of H/C, N/C, O/C and OM/OC. Because these ratios are influenced by relative organic constitutions rather than absolute organic concentrations, their diurnal patterns should be predominantly attributed to the diurnal changing of the relative importance of different sources (Huang et al., 2011). Both the O/C and OM/OC ratios reached peaks at 15:00–16:00, which is

ACPD
13, 19009–19049, 2013

when photochemistry is the most active to produce secondary organic aerosols (SOA) with high O/C ratios. Similar results were also obtained from the Pearl River Delta of China (He et al., 2011) and New York (Sun et al., 2011). However, there was an additional lower value observed at 12:00 compared with other studies. This phenomenon may have been caused by the relative contribution of the cooking source, which is the primary source with a lower O/C ratio and is higher in Beijing. The H/C ratio indicates a reverse diurnal pattern to those for O/C and OM/OC, which is as expected. However, the N/C diurnal pattern is generally consistent with the pattern of O/C and OM/OC.

Figure 3e shows a Van Krevelen diagram (H/C versus O/C) of OA using the data observed in Beijing. A significant anticorrelation (R^2 = 0.43) with a slope of −0.43 was obtained. The slope is shallower than those observed in Shenzhen (approximately −0.74) (He et al., 2011). As suggested by Heald et al. (2010), the shallower OA slope in the Van Krevelen diagram might reflect different aging mechanisms and/or the relative mixing of fresh and aged air masses in Beijing (Heald et al., 2010). On average, C, H, O, and N contributed 73.6, 7.2, 16.5 and 2.8 % to the total organic mass, respectively (Fig. 3f).

3.4 Investigating OA components/sources with positive matrix factorization (PMF)

The four organic components were identified in this campaign already discussed, including oxygenated organic aerosol (OOA), cooking-related (COA), nitrogen-containing (NOA) and hydrocarbon-like (HOA) components. Figure 4 shows the MS profiles for the four components, and Fig. 5 shows the time series for the OA components and other relevant species. PMF components were identified by their MS signatures and the correlation of their time series with tracers and then confirmed using additional information such as diurnal cycles (Zhang et al., 2005b; Ulbrich et al., 2009).

OOA have been extensively identified in previous AMS studies (Huang et al., 2011; Mohr et al., 2012; He et al., 2011) and are generally dominated by secondary organic aerosols formed in the atmosphere from gas-to-particle conversion processes of the

ACPD
13, 19009–19049, 2013

oxidation products of volatile organic compounds (Hallquist et al., 2009). The MS of the OOA component showed the characteristic features of oxidized organic material, e.g., $C_xH_yO_z$ fragments, especially CO_2^+ (m/z 44), the contribution of which reached approximately 13.5 % (Fig. 4). In many studies, this component has been divided into two subtypes according to the O/C ratios and volatilities: low-volatility OOA (LV-OOA) with higher O/C, which is more oxidized and aged, and semi-volatile OOA (SV-OOA) with lower O/C, which are less oxidized and fresher (Jimenez et al., 2009; Ng et al., 2010). In this study, we only identified the OOA the characterization of MS signatures, diurnal cycle and the ratio of O/C are close to the LV-OOA in other studies. Lanz et al. (2010) found that OOA can be separated for all summer campaigns. Slowik et al. (2010) studied an AMS winter campaign in Toronto, and Allan et al. (2010) studied three winter campaigns in Manchester and London, UK. Based on the PMF-AMS analysis, no separation of OOA into low volatility and semi volatile fractions was observed for these data. Jimenez et al. (2009) found that the relative concentrations of the OOA subtypes depended on both ambient temperature and photochemistry. For the sites with both winter and summer measurements, SV-OOA was only observed during the summer, which is when the dynamic range in ambient temperature and photochemical conditions is larger. Note that during the Payerne campaign in winter, for which LV- and SV-OOA could be differentiated, a temperature range of T ($T_{max} - T_{min}$) = 26 °C (and diurnal differences > 10 °C) was observed, which is similar to the result in Zurich summer campaign (T = 25 °C; diurnal differences > 10 °C) (Lanz et al., 2010).

The O/C ratios of the OOA identified in this campaign (0.51) were lower than the O/C ratio for the LV-OOA in other studies, such as Kaiping (0.64) (Huang et al., 2011), Shenzhen (0.59) (He et al., 2011) and New York (0.63) (Sun et al., 2011), whereas the ratios were higher than the O/C ratios for the SV-OOA of those studies (0.39, 0.45 and 0.38, respectively). The OOA time series shows a similar trend as the time series of the sulfate (R^2 = 0.91) (Fig. 5), consistent with the relationship of LV-OOA and sulfate in other studies, e.g. He et al. (2011) and DeCarlo et al. (2010). The correlation coefficient (R^2) between the OOA and two major inorganic (sulfates + nitrates) was also 0.91.

ACPD
13, 19009–19049, 2013

The strong correlation with secondary inorganic found here further supports previous evidence that OOA is predominantly secondary in its origin (Ulbrich et al., 2009). OOA displays a pronounced diurnal cycle that is characterized by a gradual increase during the daytime, with its highest contribution reaching 45.9 % at 15:00, reflecting its large photochemical production during the daytime (Fig. 6).

The COA MS extracted in this study has a lower O/C ratio (0.10) and a unique diurnal pattern. The MS of the COA is characterized by $C_xH_y^+$, especially C_nH_{2n-1}, such as *m/z* 41 (predominantly $C_3H_5^+$) and *m/z* 55 (predominantly $C_4H_7^+$), with the contributions of these tow *m/z* being 9.4 % and 9.3 %, respectively (Fig. 4). This result indicates a significant presence of unsaturated organic compounds (e.g., unsaturated fatty acids) and is consistent with the MS characteristics measured for primary Chinese cooking emissions (He et al., 2010). In addition, COA shows most significant correlation with a few $C_xH_yO_1^+$ ions, such as $C_6H_{10}O^+$ (Fig. 5), which are prominent peaks in the sources spectra of cooking emissions, thus could be used as spectral markers for COA (Sun et al., 2011). A clear and unique diurnal pattern of COA, as described by Huang et al. (2010), presented a small peak at noon and a large peak in the evening, with its highest contribution being 34.1 % at 19:00, which is in agreement with the lunch and dinner times of the local residents (Fig. 6). Due to the uniqueness of Chinese cooking habits and culture, cooking emissions have been regarded as one of the major organic aerosol sources in urban Chinese environments (He et al., 2004).

Compared with the other OA components, reports of NOA from AMS measurements are rare, which indicates a significantly higher N/C ratio (0.059) and correlates well with the N-containing ions $C_3H_8N^+$ ($R^2 = 0.66$). In the NOA MS, the highest signals were at *m/z* 29 (CHO^+) and 43 ($C_2H_3O^+$). However, the highest nitrogen-containing fragments were at *m/z* 27 (CHN^+), 29 (CH_3N^+), 30 (CH_4N^+), 41 ($C_2H_3N^+$) and 42 ($C_2H_4N^+$) (Fig. 4). The NOA of this study is similar with the NOA in New York (Sun et al., 2011) but is clearly different from the "local N-containing reduced OA" (LOA) detected in Mexico City (Aiken et al., 2009), despite the N/C ratios are similar (0.053 in New York and 0.06 in Mexico City). As the suggested by Sun et al. (2011), the mass

ACPD
13, 19009–19049, 2013

spectrum of the NOA from this study and in New York more resemble to that of the OOA, whereas the LOA in Mexico City is more similar to the HOA and biomass burning OA (BBOA). The O/C and OM/OC ratios of the NOA were 0.39 and 1.73, consistent with the ratios in New York (0.37 and 1.69) but much higher than the LOA in Mexico City (0.13 and 1.40, respectively).

It is very important to study this component deeply because the NOA in this study may contain many harmful substances. We found that NOA can be divided into four subtypes: (1) Amines, such as C_6H_7N, CH_5N, CH_2NO, CH_3NO_2, C_2H_7N and C_3H_8N. Generally, these species can be viewed as gasoline additives. Therefore, they can be emitted from motor vehicle exhaust. The concentrations of C_6H_7N and CH_5N were obviously higher than other substances. During this campaign, the average concentrations of these compounds were 0.24 $\mu g\,m^{-3}$ and 0.27 $\mu g\,m^{-3}$, with the highest values reaching 1.11 $\mu g\,m^{-3}$ and 1.50 $\mu g\,m^{-3}$, respectively. All these species accounted for 8.7 % of the NOA. (2) Urea substances. These substances can be emitted during the denitrification process in factories or power plants. The concentration of such substances in this study was 0.09 $\mu g\,m^{-3}$ (1.1 % of NOA). (3) The products of photochemical reactions. Most of these products are the decomposition products of PAN, which are typical products of the photochemical reaction. NO_2, C_2H_3O and $C_2H_3O_2$ were the main representative substances, with concentrations of 1.54 $\mu g\,m^{-3}$, 0.80 $\mu g\,m^{-3}$ and 0.01 $\mu g\,m^{-3}$, respectively. These products accounted for 32.0 % of the NOA. (4) Other nitrogen-containing substances, such as amino acids, and emissions from catering fumes.

Figure 7a and b show the NOA time series with the six major types of amines and the photochemical reaction products. The NOA correlations with these substances are significant. The range of R^2 between the NOA and NO_2, C_2H_3O and $C_2H_3O_2$ was 0.54–0.63, and the range was 0.49–0.62 between the NOA and C_6H_7N, CH_5N and CH_2NO (Fig. S4). Moreover, the diurnal variations of the NOA and the other five species were similar (the diurnal variation of $C_2H_3O_2$ was not included due to the lower content) (Fig. 7c and d). The concentrations of these species during daytime were higher than

ACPD
13, 19009–19049, 2013

at night due to photochemical production during the daytime, similar to the OOA trend. This higher value continued until the night due to the decrease in the mixing layer height. In addition to the good correlation with the NOA, these substances have a better correlation with the OOA, and the range of the correlation coefficient was R^2 = 0.63–0.78 (Fig. S5), indicating that the NOA during this campaign was the result of local source emission and regional transmission.

HOA is the most common component of OA, is predominantly attributed to primary combustion sources and has been extensively identified in previous factor analyses of AMS ambient aerosol datasets (Huang et al., 2010; Mohr et al., 2012; He et al., 2011). This component can be distinguished by the ion series of $C_nH^+_{2n+1}$ and $C_nH^+_{2n-1}$, such as $C_3H^+_5$ (m/z 41), $C_3H^+_7$ (m/z 43), $C_4H^+_7$ (m/z 55) and $C_4H^+_9$ (m/z 57), and low O/C ratios (< 0.2) (Jimenez et al., 2009; Ng et al., 2010) (Fig. 4). The lower O/C (0.1), and higher H/C (1.65) during this campaign are consistent with the results in Beijing (Huang et al., 2010) and Shanghai (Huang et al., 2012). However, the O/C ratio is higher than the values (0.03–0.04) determined for motor vehicle exhaust and the values (0.06) determined in New York (Sun et al., 2011). Similar results have also been observed in Mexico City (Aiken et al., 2009), which may indicate that the HOA identified here contains some mass from other combustion-related urban sources such as trash burning, and possibly also some lightly oxidized SOA formed from, e.g., large alkanes (Kroll et al., 2007). It is also possible that the HOA still contains some residual BBOA that was not completely separated even during the HRMS analysis, which is indicated by the signal at m/z 60 ($C_2H_4O^+_2$), often used as a tracer for BBOA (Mohr et al., 2011), and can be used to derive a levoglucosan-equivalent concentration from AMS measurements (Aiken et al., 2009). In addition, the HOA correlates well with combustion tracers such as NO_x (R^2 = 0.61) and presents a lower value during the afternoon. Together these facts indicate that the HOA is likely a surrogate for combustion POA, a conclusion reached in other studies (Aiken et al., 2009; Ulbrich et al., 2009).

The pie chart in Fig. 6 indicates that the OA mass can be explained by the PMF factors. OOA makes up 40.0 % of the OA, which is inconsistent with previous findings for

ACPD
13, 19009–19049, 2013

various locations in Northern Hemisphere midlatitudes and in central Europe (Jimenez et al., 2009; Lanz et al., 2010). The contribution of COA reached 23.4 %, making it the second largest OA component. This contribution is higher than the results from Barcelona (17 %) (Mohr et al., 2012), which is consistent with another study in Beijing (24.4 %) (Huang et al., 2010). This is an indication that cooking activities are a significant source of primary particles in Beijing and that the reasonable management of the culinary industry is very important for reducing OA in Beijing. The NOA and HOA make up 18.1 % and 18.5 % of the OA, respectively. The NOA component must be thoroughly studied because it contains many harmful substances, though the contribution is lower compared with other components.

3.5 Back trajectory clustering analysis

The Hybrid Single-Particle Lagrangian Integrated Trajectory (HYSPLIT) model is a useful air trajectory model, especially for studying the long-range transport of air masses. It has been used in many cities, such as Beijing (Huang et al., 2010; Sun et al., 2010), Shenzhen (He et al., 2011) and New York (Sun et al., 2011), to explore the influence of regional transport on PM_1 loading and composition at sampling sites.

The analysis steps in this study were similar to Huang et al. (2010). First, 48 h back trajectories starting at 500 m above ground level in Beijing (39.97°, 116.37°) were calculated every 6 h (at 00:00, 06:00, 12:00 and 18:00 LT (local time)) during the entire campaign. The trajectories were then clustered according to their similarity in a spatial distribution using the software HYSPLIT4. As a result, a five-cluster solution was adopted because of its small total spatial variance (Fig. 8). The corresponding back trajectory (BT) can be broadly classified into 4 groups based on the directions: N (cluster 2), NW (cluster 1), WNW (cluster 3 and 4), and S (cluster 5). The WNW clusters, including two important air mass types from a similar direction, were found to be the most frequent, accounting for 52 % of all BTs, followed by cluster NW (27 %), N (12 %), and S (9 %). The distribution of the transport wind direction indicated by the clusters was obviously different than the results from Beijing in summer when the most frequent

ACPD
13, 19009–19049, 2013

trajectory was from the south (Sun et al., 2010; Huang et al., 2010). For example, during the summer of 2008, southerly trajectories accounted for 46 % of all BTs, whereas the WNW trajectories accounted for 10 % (Huang et al., 2010), because the prevailing wind direction over the Beijing area during the summer is south to southeasterly, especially during the daytime. However, the weather is always influenced by a large-scale synoptic system coming from the northwest during the winter (Hu et al., 2005).

Figure 8 also shows the averaged NR-PM_1 chemical compositions corresponding to the BTs in each cluster. The WNW clusters represent the most polluted air mass origin with a mean total NR-PM_1 mass concentration of 237 $\mu g\,m^{-3}$ followed by cluster S (88.5 $\mu g\,m^{-3}$), NW (61.1 $\mu g\,m^{-3}$), and N (17.3 $\mu g\,m^{-3}$), which is because WNW clusters passed over a major coal producing area, Datong in Shanxi province, famous for abundant coal resources. Moreover, air masses in these clusters also passed over some heavily polluting industrial areas around Beijing before arriving at the sampling site. These factories were moved from Beijing in 2008 for the 29th Olympic Games. The situation for S cluster is similar to that of WNW cluster but not identical. The air mass in this cluster passed over some cities in the Shandong and Hebei provinces, such as Jinan, Dezhou and Cangzhou. Therefore, the pollutants carried by this air mass predominantly emit from these cities but not from industrial areas, which indicates high proportion of nitrates in this air mass.

The composition of every component was also different in the five clusters. Compared with other cluster, there was a larger contribution from local, primary aerosol emissions, such as COA and HOA, in N cluster. In particular, the contribution of COA reached 24.0 %. However, with the counterclockwise rotation, the contribution of local, primary aerosol emissions were decreased, and the contributions of some secondary regional aerosol constituents, such as sulfate, nitrate, chloride, ammonium and OOA, were increased, in particular, the contribution of nitrate, which was only 7.8 % in N cluster but reached 22.0 % in S cluster. Similar conclusions were obtained in a Q-AMS study in Beijing in the summer of 2006 (Sun et al., 2010) and based on a HR-ToF-AMS in Beijing during the summer of 2008.

ACPD
13, 19009–19049, 2013

To examine the contribution of different clusters during this campaign in more detail, we chose two different stages representing the lower and higher NR-PM_1 with corresponding time periods of 00:00 on 15 January to 00:00 on 22 January (period I) and 00:00 on 25 January to 00:00 on 1 February (period II). We found no obvious changes for the contribution of the cluster 5 to pollution aggravation (Fig. 9). However, the contributions of the cluster 1, 2 and 4 were decreased, especially for the cluster 2. Meanwhile, the contribution of the cluster 3 was obviously increased indicating that when the NR-PM_1 concentration was at a lower level, all the clusters contributed to the NR-PM_1 at the sampling site and that the contribution proportions were not significantly different. The contribution of the more polluted cluster 3 increased from 21.4 % to 51.0 % when the NR-PM_1 was at a higher level. Although the contribution of cluster 4, which has the same direction as the cluster 3, decreased by 8 %. Meanwhile, the contribution of the clean cluster 2 decreased to 1.4 %.

4 Conclusions

Non-refractory submicron particles (NR-PM_1) were measured in situ using a High-Resolution Time-of-Flight Aerosol Mass Spectrometer during a serious pollution month (January 2013) in a field intensive study in Beijing. On average, organics were the most abundant NR-PM_1 components, accounting for 49.8 % of the total mass, followed by sulfate (21.4 %), nitrate (14.6 %), ammonium (10.4 %), and chloride (3.8 %). The percent contribution of sulfate and nitrate increased significantly with total NR-PM_1 loading. In contrast, the percent contributions of organics decreased with total NR-PM_1 loading. The average size distributions of all components were very similar and characterized by a prominent accumulation mode peaking at 600 nm, and the organics were characterized by an additional smaller mode at ~ 200 nm. Calculations of the organic elemental composition indicate that, on average, C, H, O and N contributed to 73.6, 7.2, 16.5 and 2.8 % of the total atomic numbers of OA, respectively. The average H/C,

ACPD
13, 19009–19049, 2013

O/C and N/C (molar ratio) were 1.44, 0.34, and 0.015, respectively, corresponding to an OM/OC ratio (mass ratio of organic matter to organic carbon) of 1.60.

Positive matrix factorization (PMF) analyses of this high-resolution organic mass spectral data set identified four organic components, including oxygenated organic aerosols (OOA), cooking-related (COA), nitrogen-containing (NOA) and hydrocarbon-like (HOA), which, on average, accounted for 40.0, 23.4, 18.1 and 18.5 % of the total organic mass, respectively. NOA was identified as a dangerous signal because it included some harmful species. Back trajectory clustering analysis indicated that air masses from the south contained aerosols with a dominant fraction of secondary inorganic and organic materials. However, air masses from the north were dominated by organic material and most of the organic mass was accounted for by primary HOA and COA sources.

Supplementary material related to this article is available online at: http://www.atmos-chem-phys-discuss.net/13/19009/2013/acpd-13-19009-2013-supplement.pdf.

Acknowledgements. This study supported by the "Strategic Priority Research Program" of the Chinese Academy of Sciences (XDA05100100 & XDB05020000) and the National Natural Science Foundation of China (NO.41230642, 41175107 and 41275139). We gratefully acknowledge these financial supports.

References

Aiken, A. C., DeCarlo, P. F., Kroll, J. H., Worsnop, D. R., Huffman, J. A., D., K. S., Ulbrich, I. M., Mohr, C., Kimmel, J. R., S., D., Sun, Y., Zhang, Q., Trimborn, A., Northway, M., Z., P. J., Canagaratna, M. R., Onasch, T. B., Alfarra, M. R., P., A. S. H., Dommen, J., Duplissy, J., Metzger, A., and Baltensperger, U., and Jimenez, J. L.: O/C and OM/OC ratios of primary,

ACPD
13, 19009–19049, 2013

secondary, and ambient organic aerosols with high-resolution time-of-flight aerosol mass spectrometry, Environ. Sci. Technol., 42, 4478–4485, 2008.

Aiken, A. C., Salcedo, D., Cubison, M. J., Huffman, J. A., DeCarlo, P. F., Ulbrich, I. M., Docherty, K. S., Sueper, D., Kimmel, J. R., Worsnop, D. R., Trimborn, A., Northway, M., Stone, E. A., Schauer, J. J., Volkamer, R. M., Fortner, E., de Foy, B., Wang, J., Laskin, A., Shutthanandan, V., Zheng, J., Zhang, R., Gaffney, J., Marley, N. A., Paredes-Miranda, G., Arnott, W. P., Molina, L. T., Sosa, G., and Jimenez, J. L.: Mexico City aerosol analysis during MILAGRO using high resolution aerosol mass spectrometry at the urban supersite (T0) – Part 1: Fine particle composition and organic source apportionment, Atmos. Chem. Phys., 9, 6633–6653, doi:10.5194/acp-9-6633-2009, 2009.

Alfarra, M. R., Coe, H., Allan, J. D., Bower, K. N., Boudries, H., Canagaratna, M. R., Jimenez, J. L., Jayne, J. T., Garforth, A. A., Li, S.-M., and Worsnop, D. R.: Characterization of urban and rural organic particulate in the lower Fraser Valley using two aerodyne aerosol mass spectrometers, Atmos. Environ. , 38, 5745–5758, 2004.

Allan, J. D., Bower, K. N., Coe, H., Boudries, H., Jayne, J. T., Canagaratna, M. R., Millet, D. B., Goldstein, A. H., Quinn, P. K., Weber, R. J., and Worsnop, D. R.: Submicron aerosol composition at Trinidad Head, California, during ITCT 2K2: its relationship with gas phase volatile organic carbon and assessment of instrument performance, J. Geophys. Res.-Atmos., 109, D23S24, doi:10.1029/2003jd004208, 2004.

Allan, J. D., Delia, A. E., Coe, H., Bower, K. N., Alfarra, M. R., Jimenez, J. L., Middlebrook, A. M., Drewnick, F., Onasch, T. B., Canagaratna, M. R., Jayne, J. T., and Worsnop, D. R.: A generalised method for the extraction of chemically resolved mass spectra from aerodyne aerosol mass spectrometer data, J. Aerosol Sci., 35, 909–922, doi:10.1016/j.jaerosci.2004.02.007, 2004.

Allan, J. D., Williams, P. I., Morgan, W. T., Martin, C. L., Flynn, M. J., Lee, J., Nemitz, E., Phillips, G. J., Gallagher, M. W., and Coe, H.: Contributions from transport, solid fuel burning and cooking to primary organic aerosols in two UK cities, Atmos. Chem. Phys., 10, 647–668, doi:10.5194/acp-10-647-2010, 2010.

Beijing Statistical Yearbook 2012, Beijing Municipal Statistics Bureau, China Statistics, Beijing, China, 2012.

Brock, C. A., Sullivan, A. P., Peltier, R. E., Weber, R. J., Wollny, A., de Gouw, J. A., Middlebrook, A. M., Atlas, E. L., Stohl, A., Trainer, M. K., Cooper, O. R., Fehsenfeld, F. C., Frost, G. J., Holloway, J. S., Hübler, G., Neuman, J. A., Ryerson, T. B., Warneke, C., and

ACPD
13, 19009–19049, 2013

Wilson, J. C.: Sources of particulate matter in the northeastern United States in summer: 2. Evolution of chemical and microphysical properties, J. Geophys. Res., 113, D08302, doi:10.1029/2007jd009241, 2008.

Canagaratna, M. R., Jayne, J. T., Jimenez, J. L., Allan, J. D., Alfarra, M. R., Zhang, Q., Onasch, T. B., Drewnick, F., Coe, H., Middlebrook, A., Delia, A., Williams, L. R., Trimborn, A. M., Northway, M. J., DeCarlo, P. F., Kolb, C. E., Davidovits, P., and Worsnop, D. R.: Chemical and microphysical characterization of ambient aerosols with the aerodyne aerosol mass spectrometer, Mass Spectrom. Rev., 26, 185–222, doi:10.1002/mas.20115, 2007.

DeCarlo, P. F., Kimmel, J. R., Trimborn, A., Northway, M. J., Jayne, J. T., Aiken, A. C., Gonin, M., Fuhrer, K., Horvath, T., Docherty, K. S., Worsnop, D. R., and Jimenez, J. L.: Field-deployable, high-resolution, time-of-flight aerosol mass spectrometer, Anal. Chem., 78, 8281–8289, 2006.

DeCarlo, P. F., Ulbrich, I. M., Crounse, J., de Foy, B., Dunlea, E. J., Aiken, A. C., Knapp, D., Weinheimer, A. J., Campos, T., Wennberg, P. O., and Jimenez, J. L.: Investigation of the sources and processing of organic aerosol over the Central Mexican Plateau from aircraft measurements during MILAGRO, Atmos. Chem. Phys., 10, 5257–5280, doi:10.5194/acp-10-5257-2010, 2010.

Drewnick, F., Schwab, J. J., Jayne, J. T., Canagaratna, M., Worsnop, D. R., and Demerjian, K. L.: Measurement of ambient aerosol composition during the PMTACS-NY 2001 using an aerosol mass spectrometer, Part I: Mass concentrations, special issue of aerosol science and technology on findings from the fine particulate matter supersites program, Aerosol Sci. Tech., 38, 92–103, 2004.

Drewnick, F., Hings, S. S., DeCarlo, P., Jayne, J. T., Gonin, M., Fuhrer, K., Weimer, S., Jimenez, J. L., Demerjian, K. L., Borrmann, S., and Worsnop, D. R.: A new Time-of-Flight Aerosol Mass Spectrometer (TOF-AMS) – instrument description and first field deployment, Aerosol Sci. Tech., 39, 637–658, 2005.

Farmer, D. K., Matsunaga, A., Docherty, K. S., Surratt, J. D., Seinfeld, J. H., Ziemann, P. J., and Jimenez, J. L.: Response of an aerosol mass spectrometer to organonitrates and organosulfates and implications for atmospheric chemistry, P. Natl. Acad. Sci. USA, 107, 6670–6675, 2010.

Ge, X., Setyan, A., Sun, Y., and Zhang, Q.: Primary and secondary organic aerosols in Fresno, California during wintertime: results from high resolution aerosol mass spectrometry, J. Geophys. Res., 117, D19301, doi:10.1029/2012jd018026, 2012.

ACPD
13, 19009–19049, 2013

Ghan, S. J. and Schwartz, S. E.: Aerosol properties and processes: a path from field and laboratory measurements to global climate models, B. Am. Meteorol. Soc. , 88, 1059–1083, 2007.

Goldstein, A. H. and Galbally, I. E.: Known and unexplored organic constituents in the Earth's atmosphere, Environ. Sci. Technol., 41, 1514–1521, 2007.

Hallquist, M., Wenger, J. C., Baltensperger, U., Rudich, Y., Simpson, D., Claeys, M., Dommen, J., Donahue, N. M., George, C., Goldstein, A. H., Hamilton, J. F., Herrmann, H., Hoffmann, T., Iinuma, Y., Jang, M., Jenkin, M. E., Jimenez, J. L., Kiendler-Scharr, A., Maenhaut, W., McFiggans, G., Mentel, Th. F., Monod, A., Prévôt, A. S. H., Seinfeld, J. H., Surratt, J. D., Szmigielski, R., and Wildt, J.: The formation, properties and impact of secondary organic aerosol: current and emerging issues, Atmos. Chem. Phys., 9, 5155–5236, doi:10.5194/acp-9-5155-2009, 2009.

He, L.-Y., Hu, M., Huang, X.-F., Yu, B.-D., Zhang, Y.-H., and Liu, D.-Q.: Measurement of emissions of fine particulate organic matter from Chinese cooking, Atmos. Environ. , 38, 6557–6564, 2004.

He, L.-Y., Lin, Y., Huang, X.-F., Guo, S., Xue, L., Su, Q., Hu, M., Luan, S.-J., and Zhang, Y.-H.: Characterization of high-resolution aerosol mass spectra of primary organic aerosol emissions from Chinese cooking and biomass burning, Atmos. Chem. Phys., 10, 11535–11543, doi:10.5194/acp-10-11535-2010, 2010.

He, L.-Y., Huang, X.-F., Xue, L., Hu, M., Lin, Y., Zheng, J., Zhang, R., and Zhang, Y.-H.: Submicron aerosol analysis and organic source apportionment in an urban atmosphere in Pearl River Delta of China using high-resolution aerosol mass spectrometry, J. Geophys. Res., 116, D12304, doi:10.1029/2010jd014566, 2011.

Heald, C. L., Kroll, J. H., Jimenez, J. L., Docherty, K. S., DeCarlo, P. F., Aiken, A. C., Chen, Q., Martin, S. T., Farmer, D. K., and Artaxo, P.: A simplified description of the evolution of organic aerosol composition in the atmosphere, Geophys. Res. Lett., 37, L08803, doi:10.1029/2010gl042737, 2010.

Hu, X. M., Liu, S. H., Liang, F. M., Liu, H. P., Wang, Y. C., and Li, J.: Observational study of wind fields, temperature fields over beijing area in summer and winter, Acta Sci. Nat. Univ. Pekinensis, 41, 399–407, 2005.

Huang, X.-F., He, L.-Y., Hu, M., and Zhang, Y.-H.: Annual variation of particulate organic compounds in $PM_{2.5}$ in the urban atmosphere of Beijing, Atmos. Environ. , 40, 2449–2458, 2006.

ACPD
13, 19009–19049, 2013

Huang, X.-F., He, L.-Y., Hu, M., Canagaratna, M. R., Sun, Y., Zhang, Q., Zhu, T., Xue, L., Zeng, L.-W., Liu, X.-G., Zhang, Y.-H., Jayne, J. T., Ng, N. L., and Worsnop, D. R.: Highly time-resolved chemical characterization of atmospheric submicron particles during 2008 Beijing Olympic Games using an Aerodyne High-Resolution Aerosol Mass Spectrometer, Atmos. Chem. Phys., 10, 8933–8945, doi:10.5194/acp-10-8933-2010, 2010.

Huang, X. F., He, L. Y., Hu, M., Canagaratna, M. R., Kroll, J. H., Ng, N. L., Zhang, Y. H., Lin, Y., Xue, L., Sun, T. L., Liu, X. G., Shao, M., Jayne, J. T., and Worsnop, D. R.: Characterization of submicron aerosols at a rural site in Pearl River Delta of China using an Aerodyne High-Resolution Aerosol Mass Spectrometer, Atmos. Chem. Phys., 11, 1865–1877, doi:10.5194/acp-11-1865-2011, 2011.

Huang, X.-F., He, L.-Y., Xue, L., Sun, T.-L., Zeng, L.-W., Gong, Z.-H., Hu, M., and Zhu, T.: Highly time-resolved chemical characterization of atmospheric fine particles during 2010 Shanghai World Expo, Atmos. Chem. Phys., 12, 4897–4907, doi:10.5194/acp-12-4897-2012, 2012.

Jayne, J. T., Leard, D. C., Zhang, X., Davidovits, P., Smith, K. A., Kolb, C. E., and Worsnop, D. R.: Development of an Aerosol Mass Spectrometer for size and composition analysis of submicron particles, Aerosol. Sci. Tech., 33, 49–70, 2000.

Jimenez, J. L.: Ambient aerosol sampling using the Aerodyne Aerosol Mass Spectrometer, J. Geophys. Res., 108, 8425, doi:10.1029/2001jd001213, 2003.

Jimenez, J. L., Canagaratna, M. R., Donahue, N. M., Prevot, A. S., Zhang, Q., Kroll, J. H., DeCarlo, P. F., Allan, J. D., Coe, H., Ng, N. L., Aiken, A. C., Docherty, K. S., Ulbrich, I. M., Grieshop, A. P., Robinson, A. L., Duplissy, J., Smith, J. D., Wilson, K. R., Lanz, V. A., Hueglin, C., Sun, Y. L., Tian, J., Laaksonen, A., Raatikainen, T., Rautiainen, J., Vaattovaara, P., Ehn, M., Kulmala, M., Tomlinson, J. M., Collins, D. R., Cubison, M. J., Dunlea, E. J., Huffman, J. A., Onasch, T. B., Alfarra, M. R., Williams, P. I., Bower, K., Kondo, Y., Schneider, J., Drewnick, F., Borrmann, S., Weimer, S., Demerjian, K., Salcedo, D., Cottrell, L., Griffin, R., Takami, A., Miyoshi, T., Hatakeyama, S., Shimono, A., Sun, J. Y., Zhang, Y. M., Dzepina, K., Kimmel, J. R., Sueper, D., Jayne, J. T., Herndon, S. C., Trimborn, A. M., Williams, L. R., Wood, E. C., Middlebrook, A. M., Kolb, C. E., Baltensperger, U., and Worsnop, D. R.: Evolution of organic aerosols in the atmosphere, Science, 326, 1525–1529, doi:10.1126/science.1180353, 2009.

Lanz, V. A., Alfarra, M. R., Baltensperger, U., Buchmann, B., Hueglin, C., and Prévôt, A. S. H.: Source apportionment of submicron organic aerosols at an urban site by factor analytical

ACPD
13, 19009–19049, 2013

modelling of aerosol mass spectra, Atmos. Chem. Phys., 7, 1503–1522, doi:10.5194/acp-7-1503-2007, 2007.

Lanz, V. A., Prévôt, A. S. H., Alfarra, M. R., Weimer, S., Mohr, C., DeCarlo, P. F., Gianini, M. F. D., Hueglin, C., Schneider, J., Favez, O., D'Anna, B., George, C., and Baltensperger, U.: Characterization of aerosol chemical composition with aerosol mass spectrometry in Central Europe: an overview, Atmos. Chem. Phys., 10, 10453–10471, doi:10.5194/acp-10-10453-2010, 2010.

Liu, Q., Sun, Y., Hu, B., Liu, Z., Akio, S., and Wang, Y.: In situ measurement of PM_1 organic aerosol in Beijing winter using a high-resolution aerosol mass spectrometer, Chinese Sci. Bull., 57, 819–826, doi:10.1007/s11434-011-4886-0, 2011.

Mohr, C., Richter, R., DeCarlo, P. F., Prévôt, A. S. H., and Baltensperger, U.: Spatial variation of chemical composition and sources of submicron aerosol in Zurich during wintertime using mobile aerosol mass spectrometer data, Atmos. Chem. Phys., 11, 7465–7482, doi:10.5194/acp-11-7465-2011, 2011.

Mohr, C., DeCarlo, P. F., Heringa, M. F., Chirico, R., Slowik, J. G., Richter, R., Reche, C., Alastuey, A., Querol, X., Seco, R., Peñuelas, J., Jiménez, J. L., Crippa, M., Zimmermann, R., Baltensperger, U., and Prévôt, A. S. H.: Identification and quantification of organic aerosol from cooking and other sources in Barcelona using aerosol mass spectrometer data, Atmos. Chem. Phys., 12, 1649–1665, doi:10.5194/acp-12-1649-2012, 2012.

Murphy, D. M., Cziczo, D. J., Froyd, K. D., Hudson, P. K., Matthew, B. M., Middlebrook, A. M., Peltier, R. E., Sullivan, A., Thomson, D. S., and Weber, R. J.: Single-particle mass spectrometry of tropospheric aerosol particles, J. Geophys. Res., 111, D23S32, doi:10.1029/2006jd007340, 2006.

Ng, N. L., Canagaratna, M. R., Zhang, Q., Jimenez, J. L., Tian, J., Ulbrich, I. M., Kroll, J. H., Docherty, K. S., Chhabra, P. S., Bahreini, R., Murphy, S. M., Seinfeld, J. H., Hildebrandt, L., Donahue, N. M., DeCarlo, P. F., Lanz, V. A., Prévôt, A. S. H., Dinar, E., Rudich, Y., and Worsnop, D. R.: Organic aerosol components observed in Northern Hemispheric datasets from Aerosol Mass Spectrometry, Atmos. Chem. Phys., 10, 4625–4641, doi:10.5194/acp-10-4625-2010, 2010.

Paatero P. and Tapper, U.: Positive matrix factorization-a nonnegative factor model with optimal utilization of error-estimates of data values, Environmetrics, 5, 111–126, 1994.

Paatero, P. and Hopke, P. K.: Discarding or downweighting high-noise variables in factor analytic models, Anal. Chim. Acta, 490, 277–289, doi:10.1016/s0003-2670(02)01643-4, 2003.

ACPD
13, 19009–19049, 2013

Saarikoski, S., Carbone, S., Decesari, S., Giulianelli, L., Angelini, F., Canagaratna, M., Ng, N. L., Trimborn, A., Facchini, M. C., Fuzzi, S., Hillamo, R., and Worsnop, D.: Chemical characterization of springtime submicrometer aerosol in Po Valley, Italy, Atmos. Chem. Phys., 12, 8401–8421, doi:10.5194/acp-12-8401-2012, 2012.

Setyan, A., Zhang, Q., Merkel, M., Knighton, W. B., Sun, Y., Song, C., Shilling, J. E., Onasch, T. B., Herndon, S. C., Worsnop, D. R., Fast, J. D., Zaveri, R. A., Berg, L. K., Wiedensohler, A., Flowers, B. A., Dubey, M. K., and Subramanian, R.: Characterization of submicron particles influenced by mixed biogenic and anthropogenic emissions using high-resolution aerosol mass spectrometry: results from CARES, Atmos. Chem. Phys., 12, 8131–8156, doi:10.5194/acp-12-8131-2012, 2012.

Slowik, J. G., Vlasenko, A., McGuire, M., Evans, G. J., and Abbatt, J. P. D.: Simultaneous factor analysis of organic particle and gas mass spectra: AMS and PTR-MS measurements at an urban site, Atmos. Chem. Phys., 10, 1969–1988, doi:10.5194/acp-10-1969-2010, 2010.

Song, Y., Zhang, Y., Xie, S., Zeng, L., Zheng, M., Salmon, L. G., Shao, M., and Slanina, S.: Source apportionment of $PM_{2.5}$ in Beijing by positive matrix factorization, Atmos. Environ., 40, 1526–1537, doi:10.1016/j.atmosenv.2005.10.039, 2006.

Streets, D. G., Fu, J. S., Jang, C. J., Hao, J., He, K., Tang, X., Zhang, Y., Wang, Z., Li, Z., Zhang, Q., Wang, L., Wang, B., and Yu, C.: Air quality during the 2008 Beijing Olympic Games, Atmos. Environ., 41, 480–492, doi:10.1016/j.atmosenv.2006.08.046, 2007.

Sun, J., Zhang, Q., Canagaratna, M. R., Zhang, Y., Ng, N. L., Sun, Y., Jayne, J. T., Zhang, X., Zhang, X., and Worsnop, D. R.: Highly time- and size-resolved characterization of submicron aerosol particles in Beijing using an Aerodyne Aerosol Mass Spectrometer, Atmos. Environ., 44, 131–140, doi:10.1016/j.atmosenv.2009.03.020, 2010.

Sun, Y., Zhang, Q., Macdonald, A. M., Hayden, K., Li, S. M., Liggio, J., Liu, P. S. K., Anlauf, K. G., Leaitch, W. R., Steffen, A., Cubison, M., Worsnop, D. R., van Donkelaar, A., and Martin, R. V.: Size-resolved aerosol chemistry on Whistler Mountain, Canada with a high-resolution aerosol mass spectrometer during INTEX-B, Atmos. Chem. Phys., 9, 3095–3111, doi:10.5194/acp-9-3095-2009, 2009.

Sun, Y.-L., Zhang, Q., Schwab, J. J., Demerjian, K. L., Chen, W.-N., Bae, M.-S., Hung, H.-M., Hogrefe, O., Frank, B., Rattigan, O. V., and Lin, Y.-C.: Characterization of the sources and processes of organic and inorganic aerosols in New York city with a high-resolution time-of-flight aerosol mass spectrometer, Atmos. Chem. Phys., 11, 1581–1602, doi:10.5194/acp-11-1581-2011, 2011.

ACPD
13, 19009–19049, 2013

Takegawa, N., Miyazaki, Y., Kondo, Y., Komazaki, Y., Miyakawa, T., Jimenez, J. L., Jayne, J. T., Worsnop, D. R., Allan, J. D., and Weber, R. J.: Characterization of an Aerodyne Aerosol Mass Spectrometer (AMS): intercomparison with other aerosol instruments, Aerosol. Sci. Tech., 39, 760–770, doi:10.1080/02786820500243404, 2005.

Takegawa, N., Miyakawa, T., Kondo, Y., Blake, D. R., Kanaya, Y., Koike, M., Fukuda, M., Komazaki, Y., Miyazaki, Y., Shimono, A., and Takeuchi, T.: Evolution of submicron organic aerosol in polluted air exported from Tokyo, Geophys. Res. Lett., 33, L15814, doi:10.1029/2006gl025815, 2006.

Takegawa, N., Miyakawa, T., Watanabe, M., Kondo, Y., Miyazaki, Y., Han, S., Zhao, Y., van Pinxteren, D., Bruggemann, E., Gnauk, T., Herrmann, H., Xiao, R., Deng, Z., Hu, M., Zhu, T., and Zhang, Y.: Performance of an Aerodyne Aerosol Mass Spectrometer (AMS) during intensive campaigns in China in the summer of 2006, Aerosol. Sci. Tech., 43, 189–204, doi:10.1080/02786820802582251, 2009.

Turpin, B. J. and Lim, H.-J.: Species contributions to $PM_{2.5}$ mass concentrations: revisiting common assumptions for estimating organic mass, Aerosol. Sci. Tech., 35, 602–610, doi:10.1080/02786820119445, 2001.

Ulbrich, I. M., Canagaratna, M. R., Zhang, Q., Worsnop, D. R., and Jimenez, J. L.: Interpretation of organic components from Positive Matrix Factorization of aerosol mass spectrometric data, Atmos. Chem. Phys., 9, 2891–2918, doi:10.5194/acp-9-2891-2009, 2009.

Volkamer, R., Jimenez, J. L., San Martini, F., Dzepina, K., Zhang, Q., Salcedo, D., Molina, L. T., Worsnop, D. R., and Molina, M. J.: Secondary organic aerosol formation from anthropogenic air pollution: rapid and higher than expected, Geophys. Res. Lett., 33, L17811, doi:10.1029/2006gl026899, 2006.

Xiao, R., Takegawa, N., Kondo, Y., Miyazaki, Y., Miyakawa, T., Hu, M., Shao, M., Zeng, L. M., Hofzumahaus, A., Holland, F., Lu, K., Sugimoto, N., Zhao, Y., and Zhang, Y. H.: Formation of submicron sulfate and organic aerosols in the outflow from the urban region of the Pearl River Delta in China, Atmos. Environ., 43, 3754–3763, doi:10.1016/j.atmosenv.2009.04.028, 2009.

Zhang, Q., Canagaratna, M. R. J., J. T., Worsnop, D. R., and Jimenez, J. L.: Time- and size-resolved chemical composition of submicron particles in Pittsburgh: implications for aerosol sources and processes, J. Geophys. Res., 110, D07S09, doi:10.1029/2004jd004649, 2005a.

ACPD
13, 19009–19049, 2013

Zhang, Q., Worsnop, D. R., Canagaratna, M. R., and Jimenez, J. L.: Hydrocarbon-like and oxygenated organic aerosols in Pittsburgh: insights into sources and processes of organic aerosols, Atmos. Chem. Phys., 5, 3289–3311, doi:10.5194/acp-5-3289-2005, 2005b.

Zhang, Q., Jimenez, J. L., Canagaratna, M. R., Allan, J. D., Coe, H., Ulbrich, I., Alfarra, M. R., Takami, A., Middlebrook, A. M., Sun, Y. L., Dzepina, K., Dunlea, E., Docherty, K., DeCarlo, P. F., Salcedo, D., Onasch, T., Jayne, J. T., Miyoshi, T., Shimono, A., Hatakeyama, S., Takegawa, N., Kondo, Y., Schneider, J., Drewnick, F., Borrmann, S., Weimer, S., Demerjian, K., Williams, P., Bower, K., Bahreini, R., Cottrell, L., Griffin, R. J., Rautiainen, J., Sun, J. Y., Zhang, Y. M., and Worsnop, D. R.: Ubiquity and dominance of oxygenated species in organic aerosols in anthropogenically-influenced Northern Hemisphere midlatitudes, Geophys. Res. Lett., 34, L13801, doi:10.1029/2007gl029979, 2007.

ACPD
13, 19009–19049, 2013

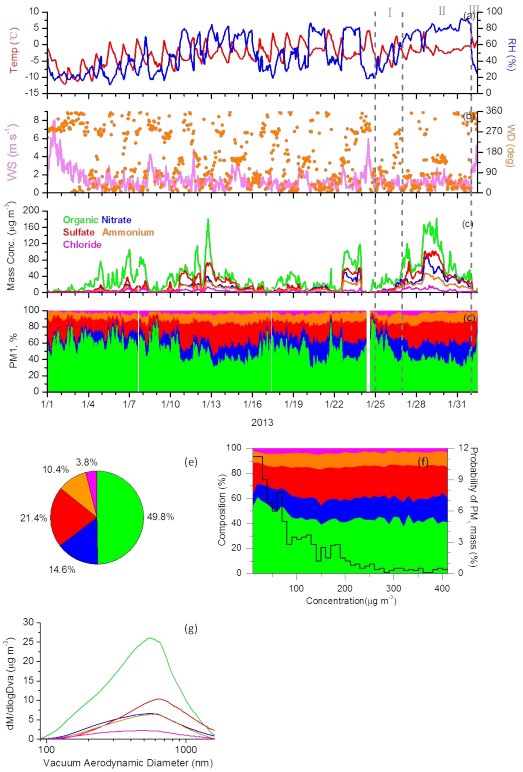

Fig. 1. Chemical compositions and size distributions of the NR-PM_1 during the campaign: time series of **(a)** ambient temperature and relative humidity; **(b)** wind direction and wind speed; **(c)** NR-PM_1 species concentrations; **(d)** NR-PM_1 percent composition; **(e)** NR-PM_1 chemical composition; **(f)** the variation of the percent composition with the NR-PM_1 mass concentration; **(g)** the average size distributions of the AMS species.

ACPD
13, 19009–19049, 2013

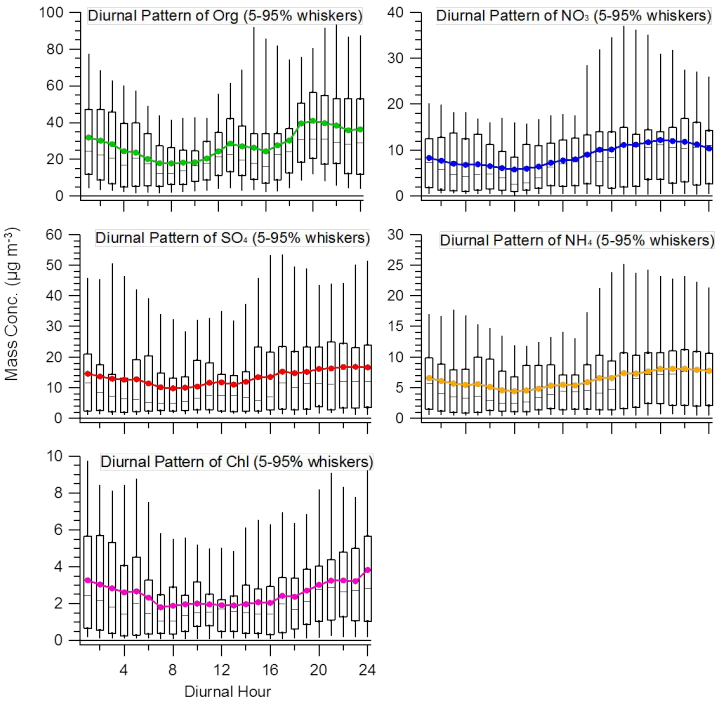

Fig. 2. Diurnal variation box plots of the NR-PM_1 species. The upper and lower boundaries of boxes indicate the 75th and 25th percentiles; the line within the box marks the median; the whiskers above and below boxes indicate the 95th and 5th percentiles; and the circle symbols represent the means.

ACPD
13, 19009–19049, 2013

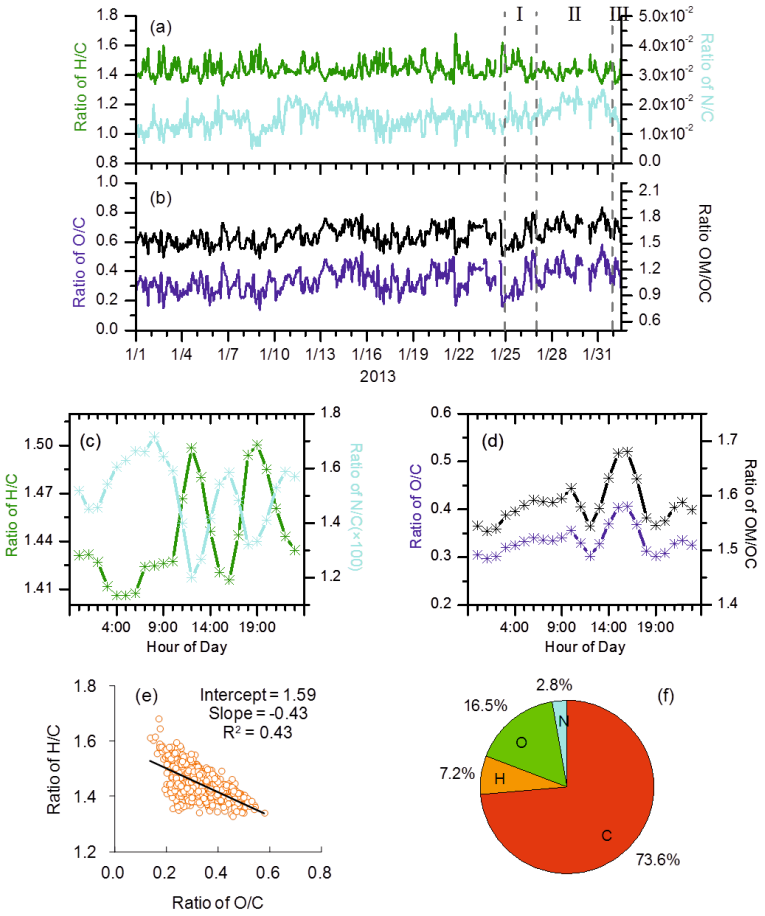

Fig. 3. The time series of **(a)** H/C and N/C ratios and **(b)** O/C and OM/OC ratios; and the average diurnal variations of **(c)** H/C and N/C ratios and **(d)** O/C and OM/OC ratios. **(e)** The Van Krevelen diagram and **(f)** the average mass-based organic elemental composition.

ACPD
13, 19009–19049, 2013

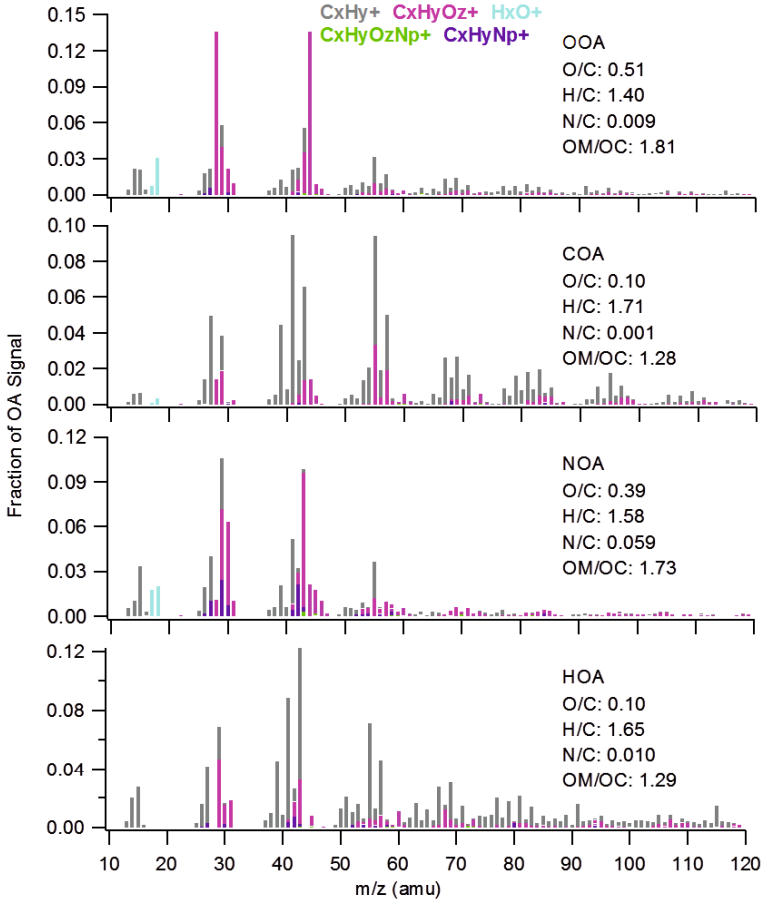

Fig. 4. The AMS m/z profiles of the four OA components identified by PMF in this study.

ACPD
13, 19009–19049, 2013

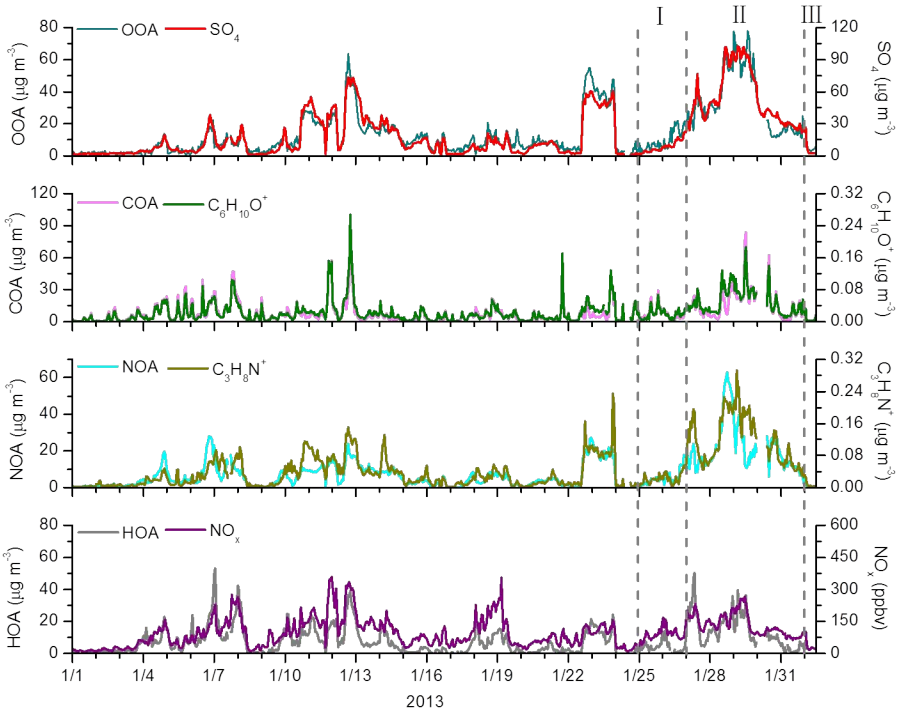

Fig. 5. Time series of the OA components and other relevant species.

ACPD
13, 19009–19049, 2013

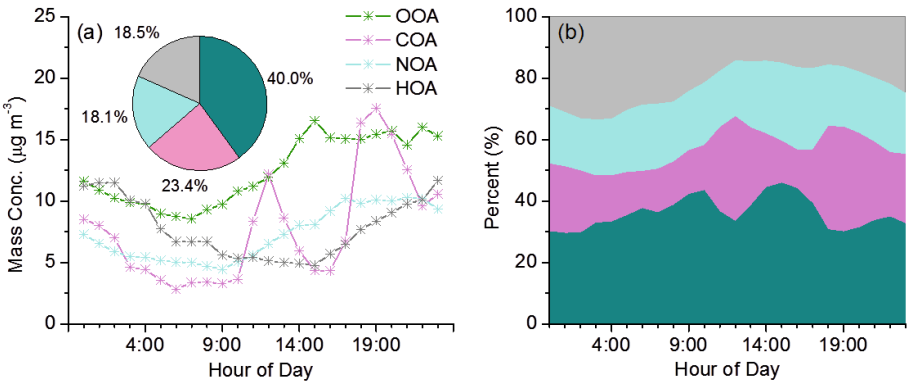

Fig. 6. (a) The diurnal variations and the average composition of the OA components and **(b)** their diurnal profiles by percent mass.

ACPD
13, 19009–19049, 2013

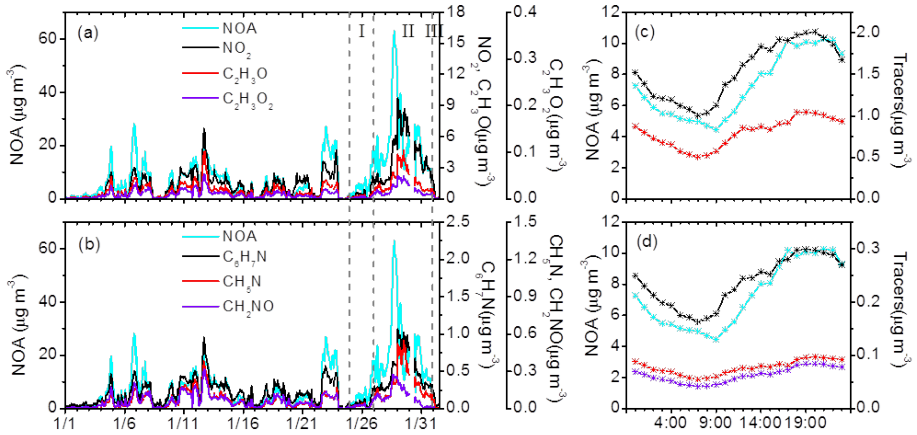

Fig. 7. Time series and diurnal variations of the NOA component and other relevant species.

ACPD
13, 19009–19049, 2013

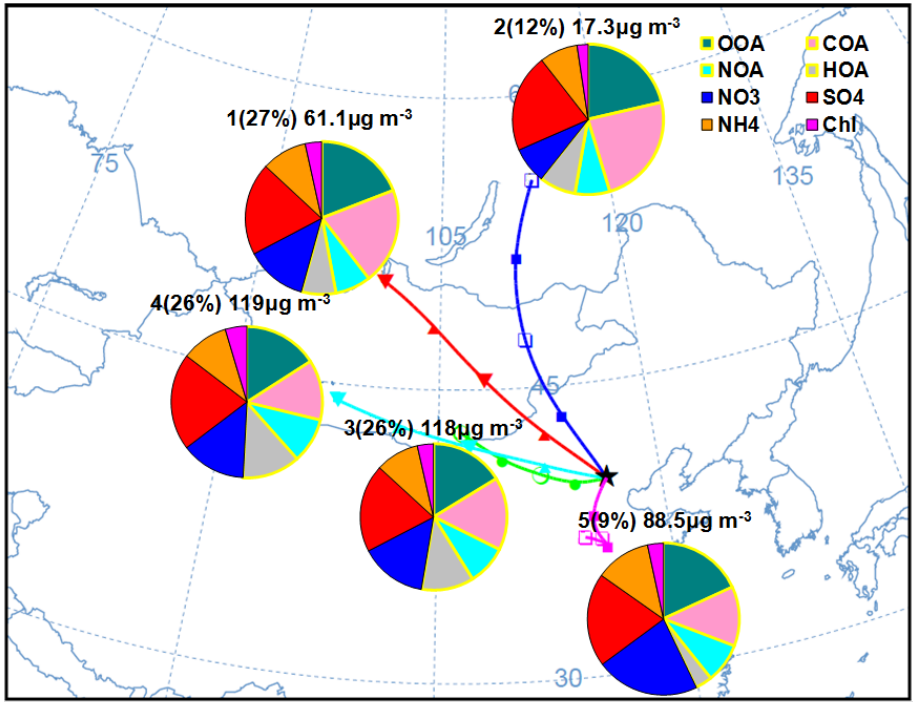

Fig. 8. Back trajectories for each of the identified clusters and corresponding cluster average NR-PM_1 compositions during the campaign.

ACPD
13, 19009–19049, 2013

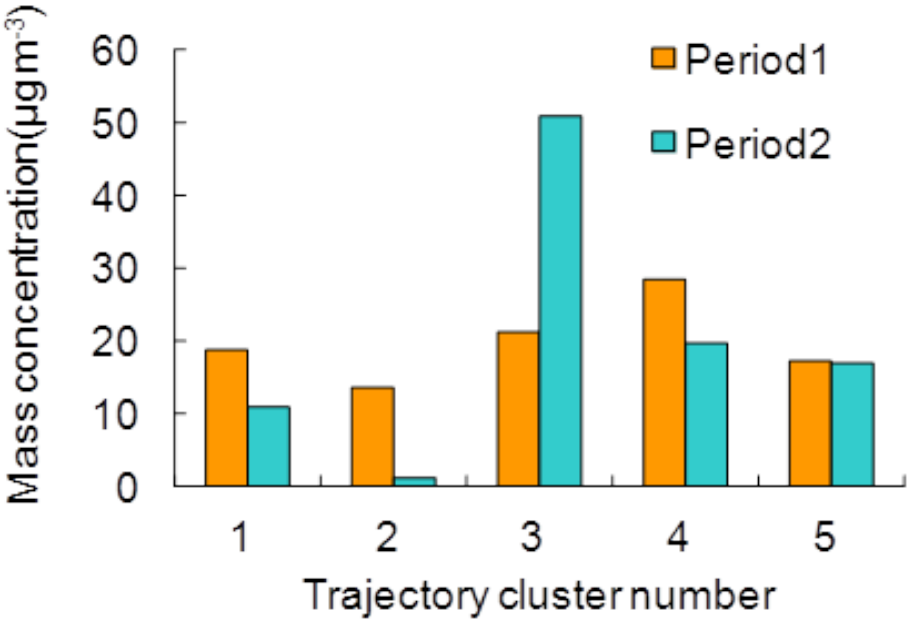

Fig. 9. The contribution of the five trajectory clusters during different stages.

ACPD
13, 19009–19049, 2013